Milankovitch cycles in REE+Y:
A new geochemical tool for cyclostratigraphic analysis of BIFs

Abstract

Spectral analysis was performed on the UU BH-1 core containing the Kuruman banded iron formation (BIF) in order to identify the presence of Milankovitch cycles. We analysed the Fe/Mn which has been found to capture Milankovitch cycles, as well as the rare-earth element + Yttrium (REE+Y) record of a ~100m section of the core. Several recurring cycles were found across all proxies examined in the form of ~3.8m, ~5.2m, ~8.0m and ~19.5m cycles. The ~8.0m cycle was found to be a double ~3.8m cycle and together with the ~5.2m cycle explains nearly all elemental variations found throughout the stratigraphy. The ~19.5m cycle most likely functions as a modulation on the ~5.2m and ~8.0m cycles as the ~8.0m cycles were found to be most dominant with a weak ~19.5m cycle in the middle of the stratigraphy. REE+Y were able to capture a distinct signal throughout the entire stratigraphy, even in sections where Fe/Mn was incapable of capturing clear cycles. The REE+Y showed an antiphase relationship with Fe/Mn while Y/Ho and La were nearly in-phase with it. Y/Ho exhibited an exceedingly high coherence (0.71-0.91) with Fe/Mn at the period considered and was found to most directly respond to changes in continental input and thus climate. Due to the agreement between the cycles found in the Fe/Mn and REE+Y record we conclude that there is a direct climatological control on REE+Y in BIFs.

1. Introduction

Banded iron formations (BIFs) are chemical marine sedimentary deposits that were deposited throughout the Archean and Paleoproterozoic under ferruginous and anoxygenic conditions (Bekker et al., 2010; Konhauser et al., 2017). Their composition provides a window into the environmental conditions of the early Earth and as such is used to study Precambrian Earth conditions and processes. The controls on BIF deposition are not yet fully understood, but a climatological control was identified in Lantink et al. (2019). Using high-precision U-Pb dating to create an average depositional rate and a spectral analysis of the weathering profile of the Kuruman formation, Lantink et al. (2019) found two periodicities of 4.3-6.3m and 12-16m corresponding with ~405 Kyr and 1.2-1.6 Ma eccentricities respectively. In Haddouzi (2019) we sampled the UU BH-1 core containing the Kuruman formation at a 1m resolution and we likewise observed recurring cycles, but in the rare-earth elements + Yttrium (REE+Y) instead. The cyclostratigraphic part of the study was qualitative in nature, but nevertheless showed that cyclicity was present in the chemical data of the Kuruman BIF. REE+Y are not commonly used in cyclostratigraphic studies, but their stability in seawater (Bekker et al., 2014) and their dependence on terrestrial input which itself is climatologically controlled (Elderfield 1981; 1988). makes them a potentially valuable tool. In order to further validate the climatological control on BIF deposition found in Lantink et al. (2019), a follow up study on Haddouzi (2019) is required. In this study we aim to quantitatively identify cyclicities in the chemical data of the Kuruman BIF and compare these to those found in Lantink et al. (2019) and unpublished data by Lantink et al., which will henceforth be referred to as Lantink et al. (unpubl.). If cycles are identified, we aim to formulate a hypothesis as to why these cycles can be found in REE+Y.

2. Methods

2.1 Data used

This study uses the bulk rock data and the REE+Y data acquired from the carbonate fraction separation performed in Haddouzi (2019). Here, a simplified version of the mineral separation scheme developed in Oonk et al. (2017) was applied in order to isolate the carbonate fraction of the Kuruman BIF, which has been found to be most representative of a primary seawater signal (Bau et al., 1996; Oonk et al., 2017; 2018). In Haddouzi (2019), the UU BH-1 core was sampled at a 1m resolution over a 100m section of the core. The datapoint at depth marker 257m has been left out of the dataset by Haddouzi (2019) to represent the loss of core between 256m and 258m. The data used from Lantink et al. (unpubl.) is bulk rock data from the same interval. The REE+Y proxies that will be used in this study are Y/Ho, Yb/Pr, sumREE (i.e. the sum of all REE+Y), Ce, La and Eu. All concentrations are in ppm.

2.2 Spectral analysis

The data was processed using the time-series analysis software Acycle (Li et al., 2019). The various datasets have been interpolated at 0.5m and detrended using locally weighted scatterplot smoothing (LOWESS). For the spectral analysis we applied the multitaper method (MTM) developed in Thomson (1982) and we subsequently applied a bandpass filtering with a Gaussian window to filter for the identified periods. Cross-spectral analysis was performed between the Fe/Mn from Lantink et al. (unpubl.) and the data from this study according to the Blackman-Tukey method (Paillard et al., 1996) using Analyseries v1.1.

3. Results

3.1 Data evaluation

The Fe/Mn of Haddouzi (2019) is in accordance with the Fe/Mn of Lantink et al. (unpubl.) displayed in figure 1. The values (i.e. concentrations) from Haddouzi (2019) are a factor 10 smaller, but the patterns are the same. Cross-spectral analysis was performed on the two Fe/Mn datasets for further comparison and can be found in figure 4. Coherency is >0.86 at periods greater than ~2.5m and is in phase from this point onward (Fig.4b and 4c). These findings combined confirm the concordance between our Fe/Mn and that measured in Lantink et al. (unpubl.).

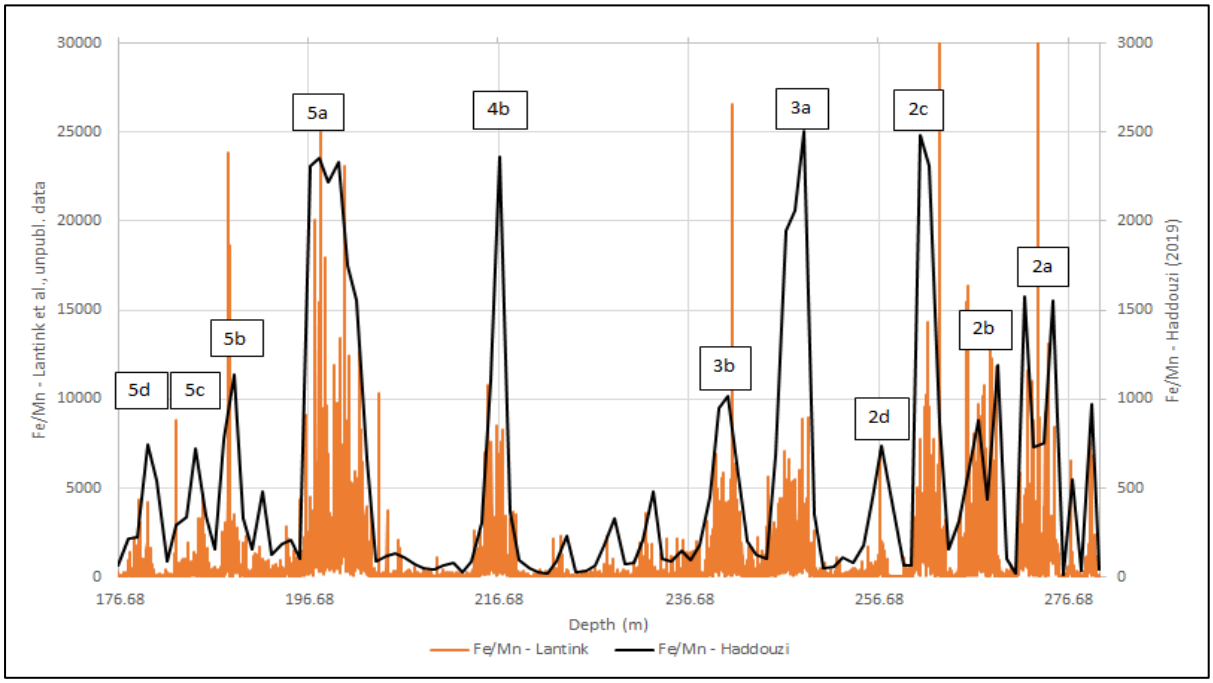

Figure 1: The Fe/Mn of this study plotted alongside the Fe/Mn from Lantink et al. (unpubl.). The hard ridges from Lantink et al. (2019; e.g. 2a, 3a, etc) have been denotated accordingly.

3.2 Fe/Mn and REE

Y/Ho and Fe/Mn from Haddouzi (2019) have been plotted in figure 2. The amplitude of Y/Ho is regular throughout the core while Fe/Mn is mostly characterised by high amplitude peaks interspersed with smaller amplitude peaks. The largest Fe/Mn peaks coincide with almost all the largest peaks found in Y/Ho. The middle part of the stratigraphy contains a regular sequence for both elements though at different places in the stratigraphy; Fe/Mn has three small peaks (Fig.2, 220-235m) that increase in magnitude with depth and a larger peak (~240m) which might also be part of this three-peak sequence. Similarly, Y/Ho has three increasing double peaks (Fig.2, 220-240m), where the difference between the larger and smaller peaks diminishes with depth.

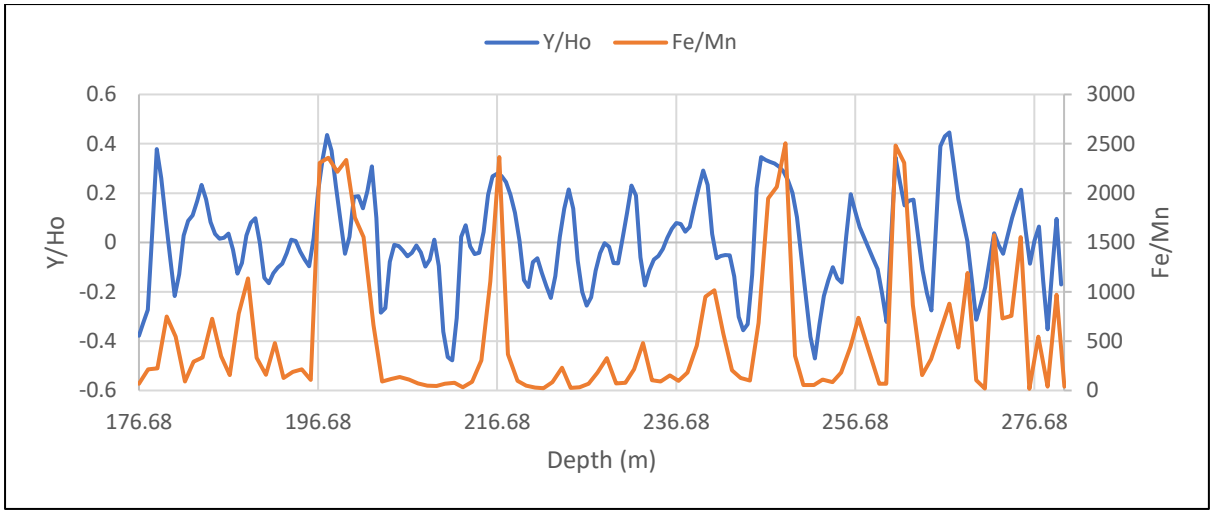

Figure 2: Y/Ho and Fe/Mn plotted against depth. Detrended Y/Ho values have been plotted.

3.3 MTM

MTM spectra were created for Fe/Mn and the REE+Y (Fig.3). The common peaks which were significant (>90% confidence) were filtered in the bandpass section together with other peaks of interest. The MTM spectra of the Fe/Mn and Y/Ho are displayed in figure 3, while the other spectra including the spectra of the Fe/Mn from Lantink et al. (unpubl.) can be found in Appendix A. The most significant bands (>95% confidence) in the Fe/Mn are at ~4.5m, ~7.1m and 15-20m. For Y/Ho, the bands that exceed this same significance level are found at ~3.7m and ~8.3m.

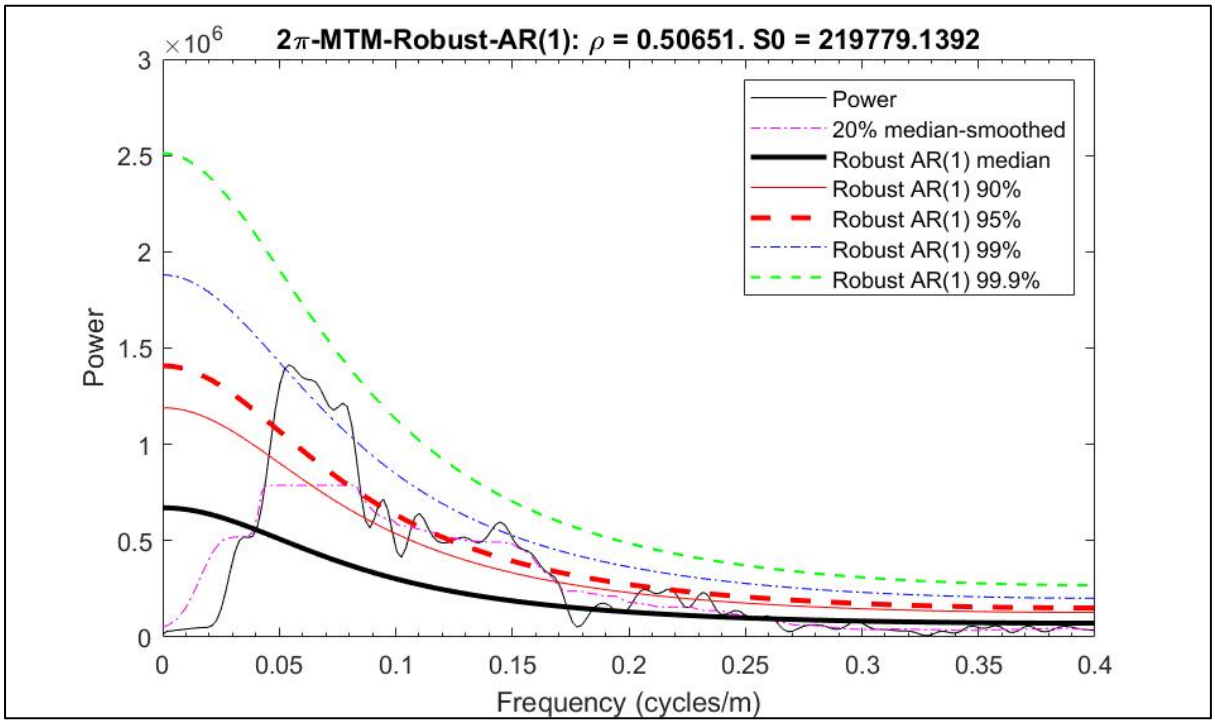

Figure 3a: MTM spectrum of Fe/Mn.

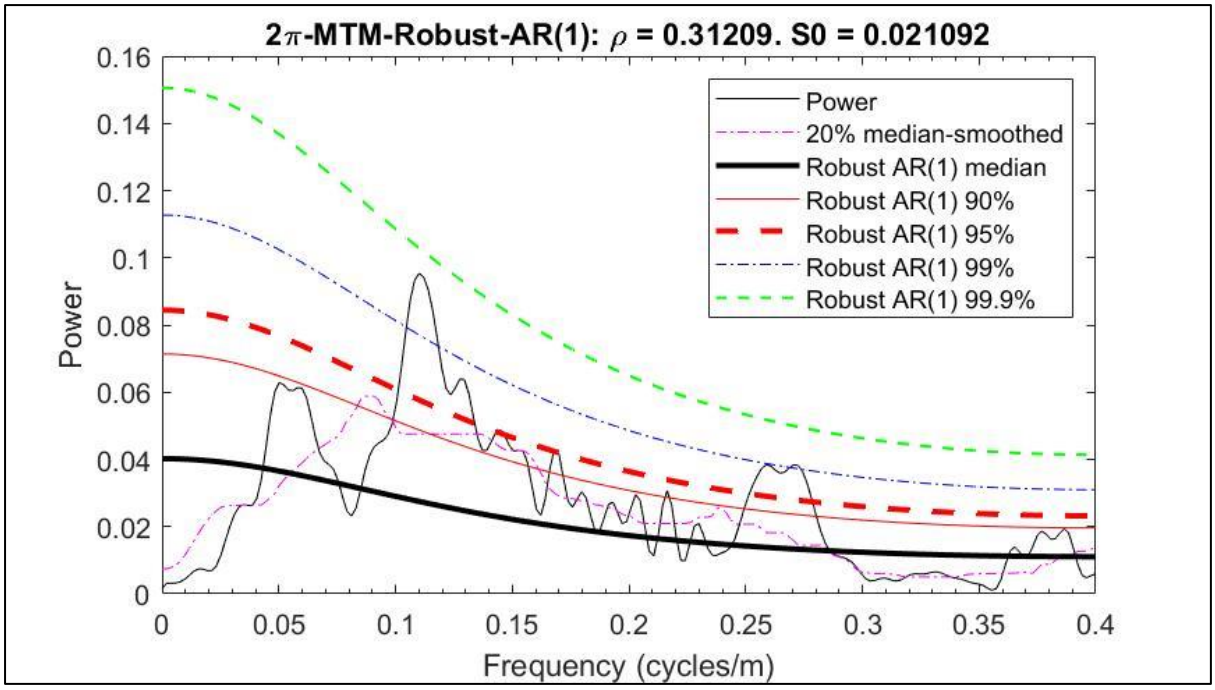

Figure 3b: MTM spectrum of Y/Ho.

3.4 Cross-Spectral analysis

The REE+Y show varying degrees of coherence and phase relationships with the Fe/Mn (Fig.5, Appendix B), with Y/Ho having the best agreement with it by a significant margin. Y/Ho exhibits a high coherence (>0.7) with the Fe/Mn at periods greater than 4m. The periods with the highest coherence (>0.80) are 6.3-8.5m and >13.4m. Y/Ho is found to be almost entirely in phase with the Fe/Mn (Fig.5c). The coherence and phase relationships of the other REE+Y while varied (Appendix B), show several trends:

- In all proxies, one of the most coherent periods is found in the ~6-8m interval.
- All proxies, except for Y/Ho and La, show an antiphase relationship with the Fe/Mn record in almost all periods.
- Except for Y/Ho, the highest coherence found in any proxy does not exceed 0.70-0.75.

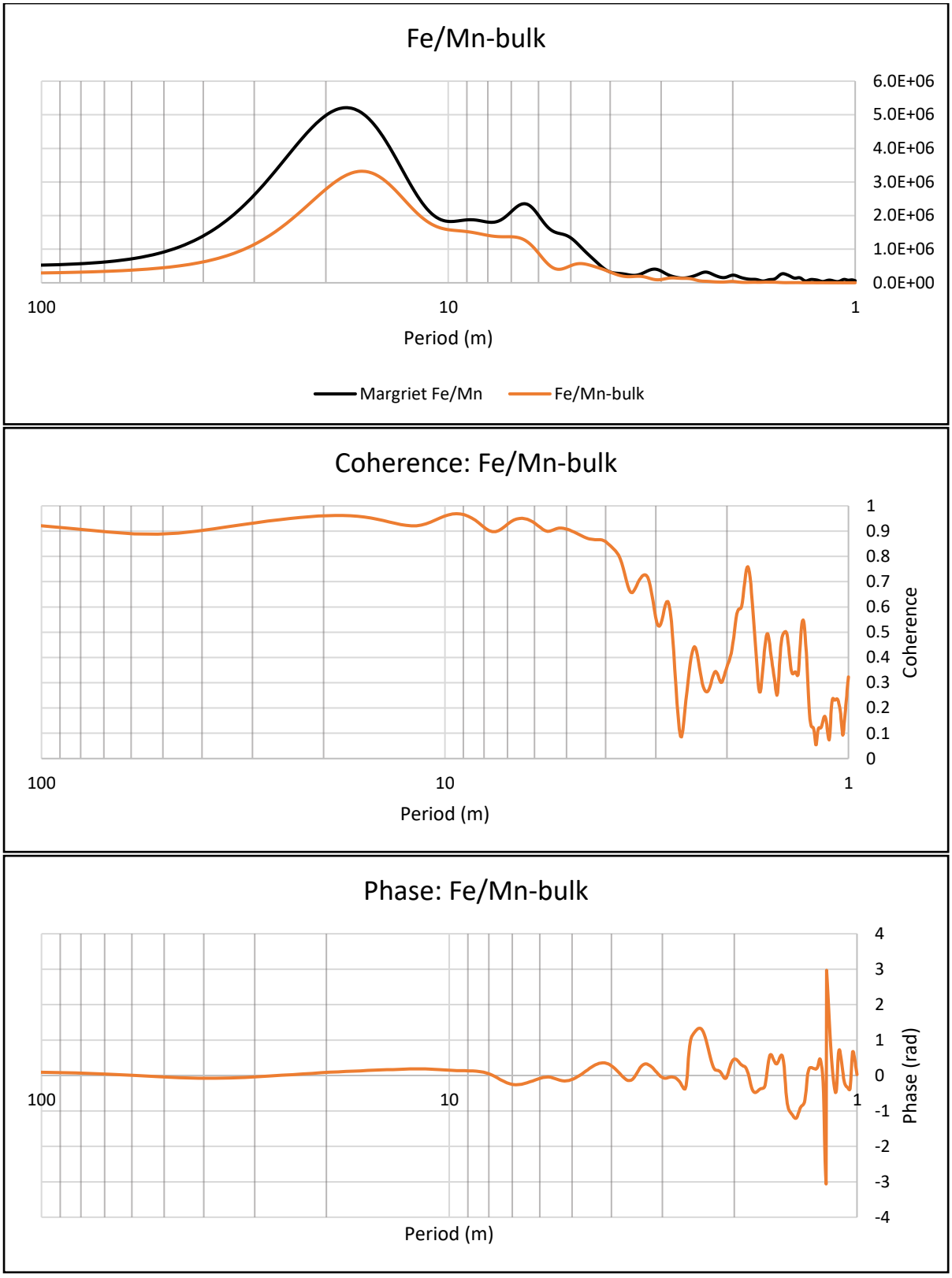

Figures 4a, b and c: (a) MTM spectrum, (b) coherence and (c) phase relationships between the Fe/Mn from this study and that of Lantink et al. (unpubl.).

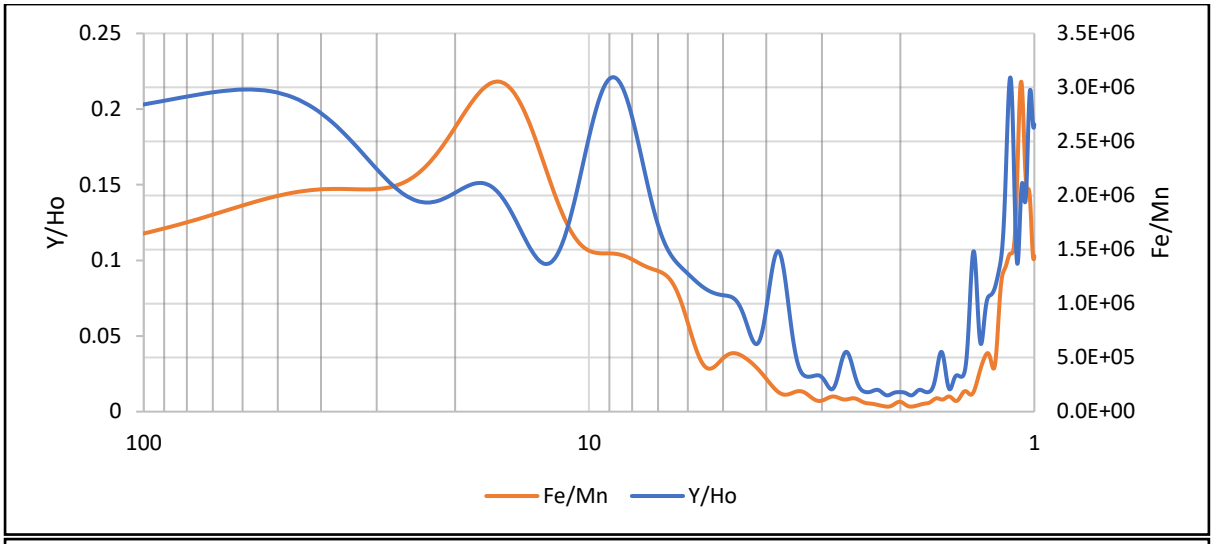

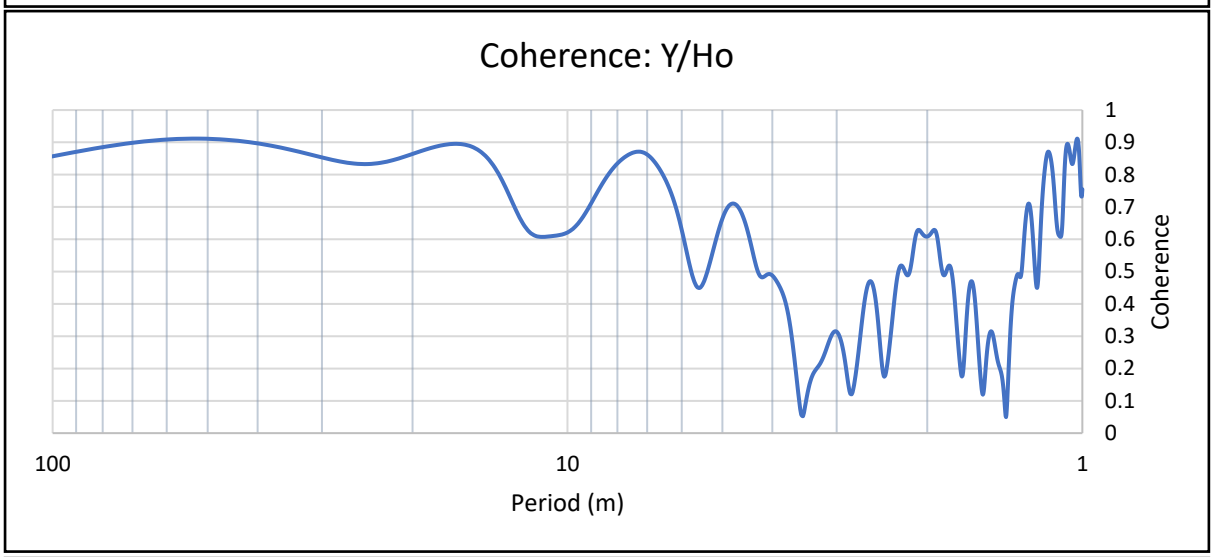

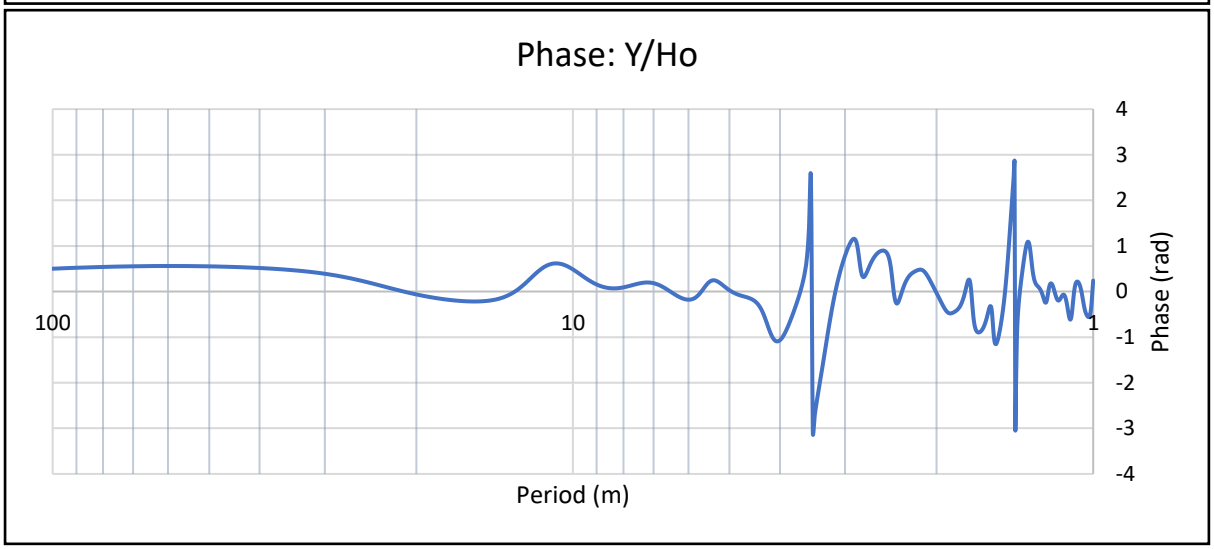

Figure 5a, b and c: (a) MTM spectrum, (b) coherence and (c) phase relationship between Fe/Mn and Y/Ho.

3.5 Bandpass filtering

A total of five cycle intervals were identified across all proxies examined and an additional cycle at ~11.4m in Fe/Mn, Yb/Pr, Ce and La (Table.1; Appendix C). The average common cycles are ~2.8m, ~3.8m, ~5.2m, ~8.om and ~19.5m. The exact cycles vary from element to element, but these averages will be used henceforth to represent the same approximate cycle interval when comparing proxies. The exact cycles filtered can be found in Table 1. The various cycles noted occur in a variety of modes depending on the element considered, but several trends can be observed. A more in-depth description of the proxies other than Fe/Mn and Y/Ho can be found in Appendix C3-C7. The ~11.3m cycles were found to not correctly follow any real element variations throughout all proxies and will therefore not be discussed.

Fe/Mn (Fig.6) – The small-scale elemental variations in the outer ends of the upper and lower stratigraphy are relatively well captured by the ~3.0m cycle. The ~3.7m is a relatively poor fit, though it is the best fit for the three small peaks in the 220-235m interval which are not captured by any other cycle. The ~4.7m and ~7.1m cycles are strong in the lower part of the stratigraphy, with the ~4.7m cycle also being notable in the upper part of the stratigraphy. The ~16.9m cycle is significant throughout with there being a weaker cycle in the middle of the stratigraphy.

Y/Ho (Fig.7) **–** The smallest peaks throughout are captured by the ~2.7m and ~3.7m cycles, while the broader peaks (e.g. 211-260) are captured by the ~8.3m cycle. The long ~17.2m cycle running through the entire profile is weakest at ~232m depth. The large cycles correspond with large Fe/Mn excursions in the Fe/Mn record. The strength of the signal for the ~2.7m and ~4.8m is most significant in the upper and lower parts of the stratigraphy, while that of the ~3.7m and ~8.3m is strongest everywhere except the lower stratigraphy.

<u>General observations</u>

- The ~2.8m and ~3.8m cycles capture most of the minor elemental variations in all proxies throughout the entire profile.
- The ~5.2m cycle is most significant in the lower part of the stratigraphy alone, or in the lower and upper stratigraphy at the same time.
- The ~8.0m cycle is relatively consistent throughout but is most significant in the middle part of the stratigraphy.
- The ~2.8m cycle is most significant in intervals where the ~5.2m cycle is significant, while the ~3.8m cycle is most significant in intervals where the ~8.0m is significant.
- The strongest or the weakest ~19.5m cycle in several proxies coincides with the middle part of the stratigraphy.

Table 1: Summary of the exact cycles identified in meters.

Y/Ho	sumREE	Yb/Pr	Ce	La	Eu	Fe/Mn	Average
2.7	2.9	2.9	2.7	2.7	2.9	3.0	2.8
3.7	3.6	4.0	3.8	3.8	3.8	3.7	3.8
4.8	5.1	5.6	5.3	5.3	5.5	4.7	5.2
8.3	8.2	8.9	8.0	6.8	8.5	7.1	8.0
N/A	N/A	10.9	11.6	11.8	N/A	11.1	11.3
17.2	20.0	21.3	19.2	20.0	21.7	16.9	19.5

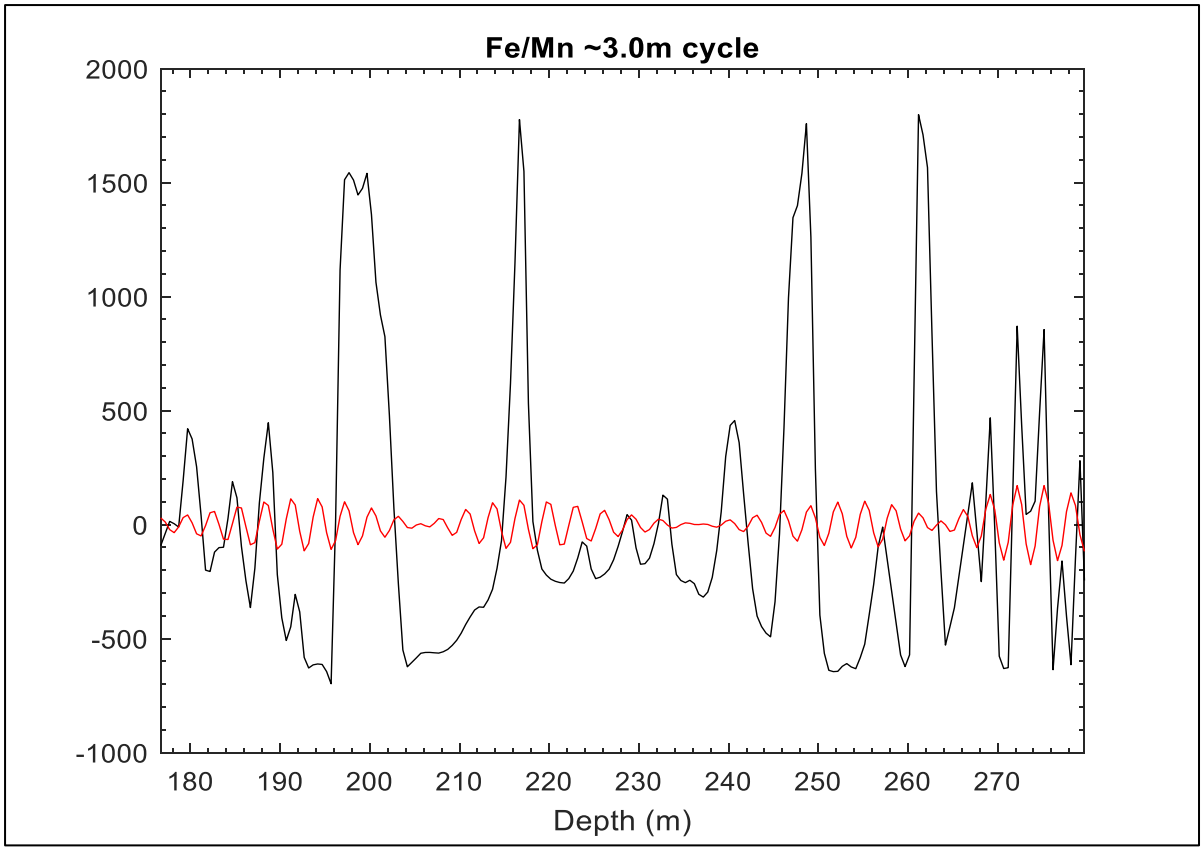

Figure 6a: The ~3.0m cycle of Fe/Mn.

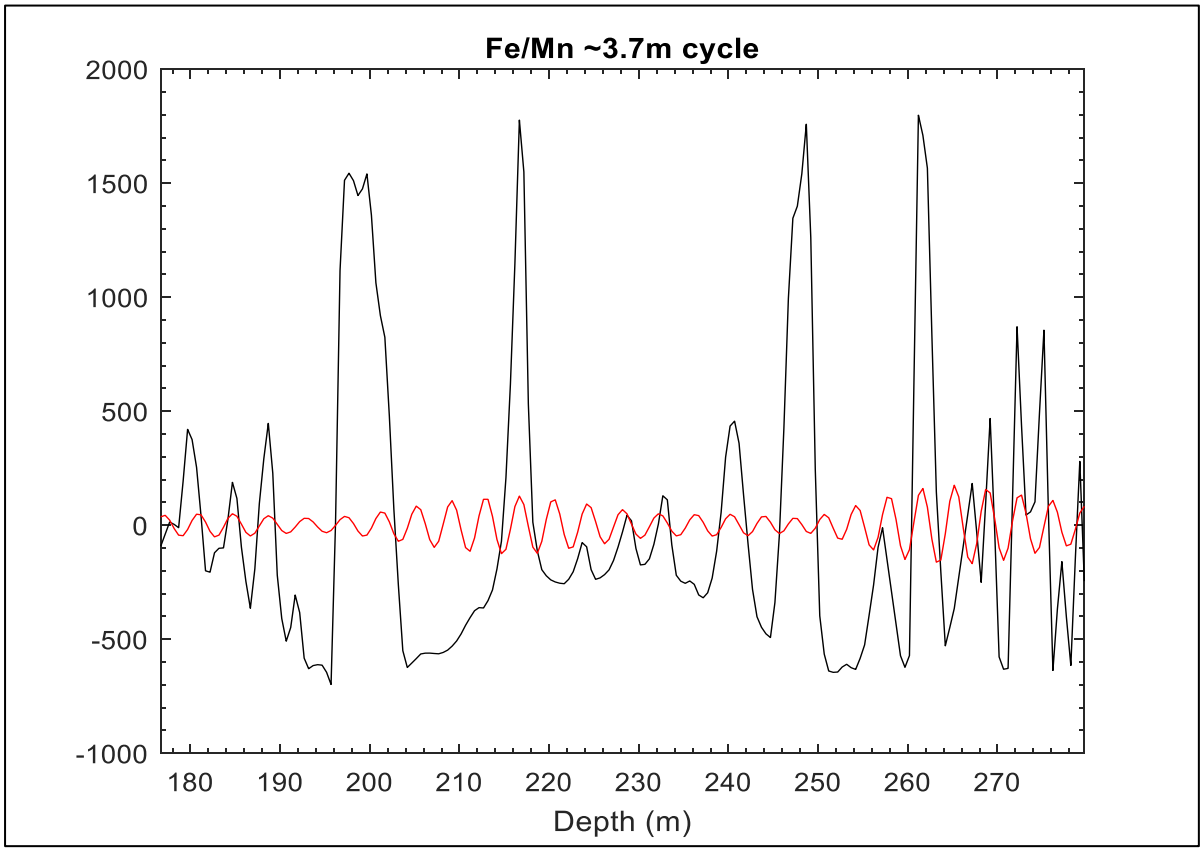

Figure 6b: The ~3.7m cycle of Fe/Mn.

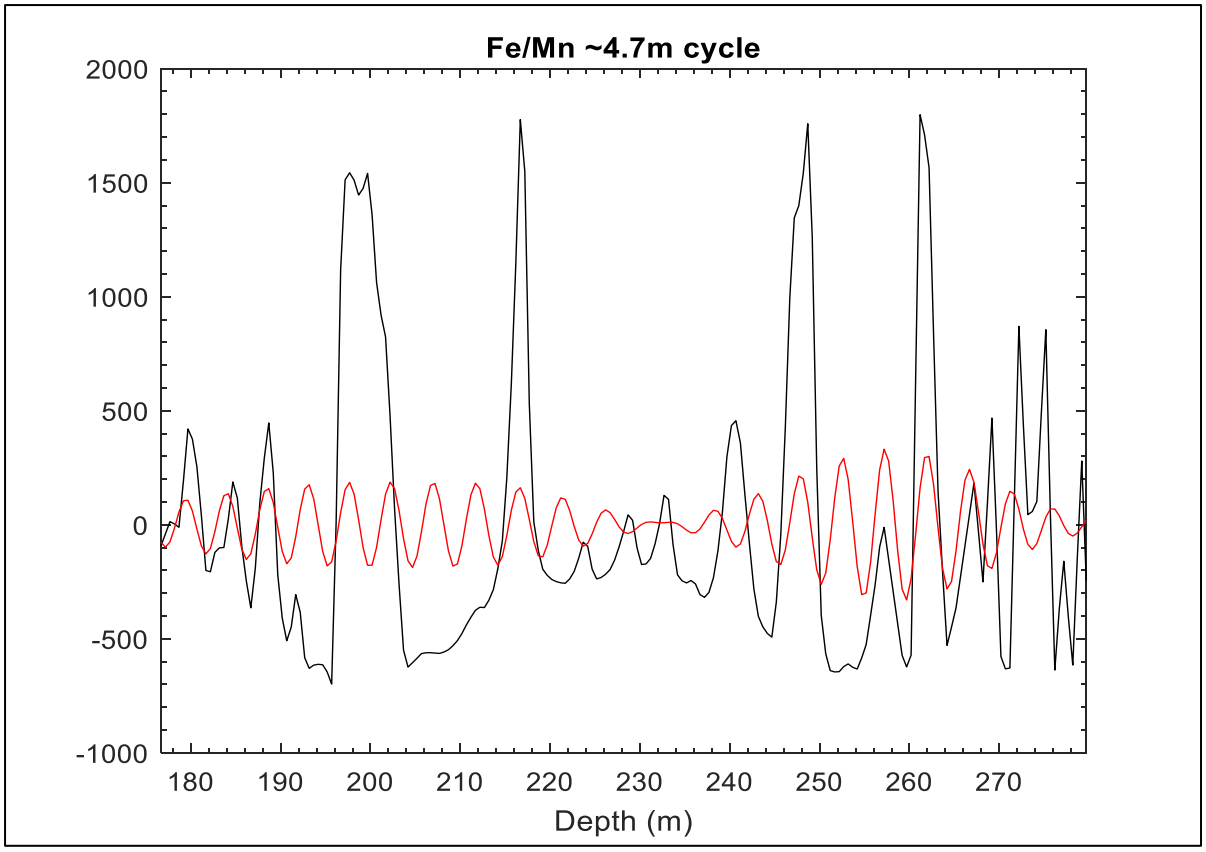

Figure 6c: The ~4.7m cycle of Fe/Mn.

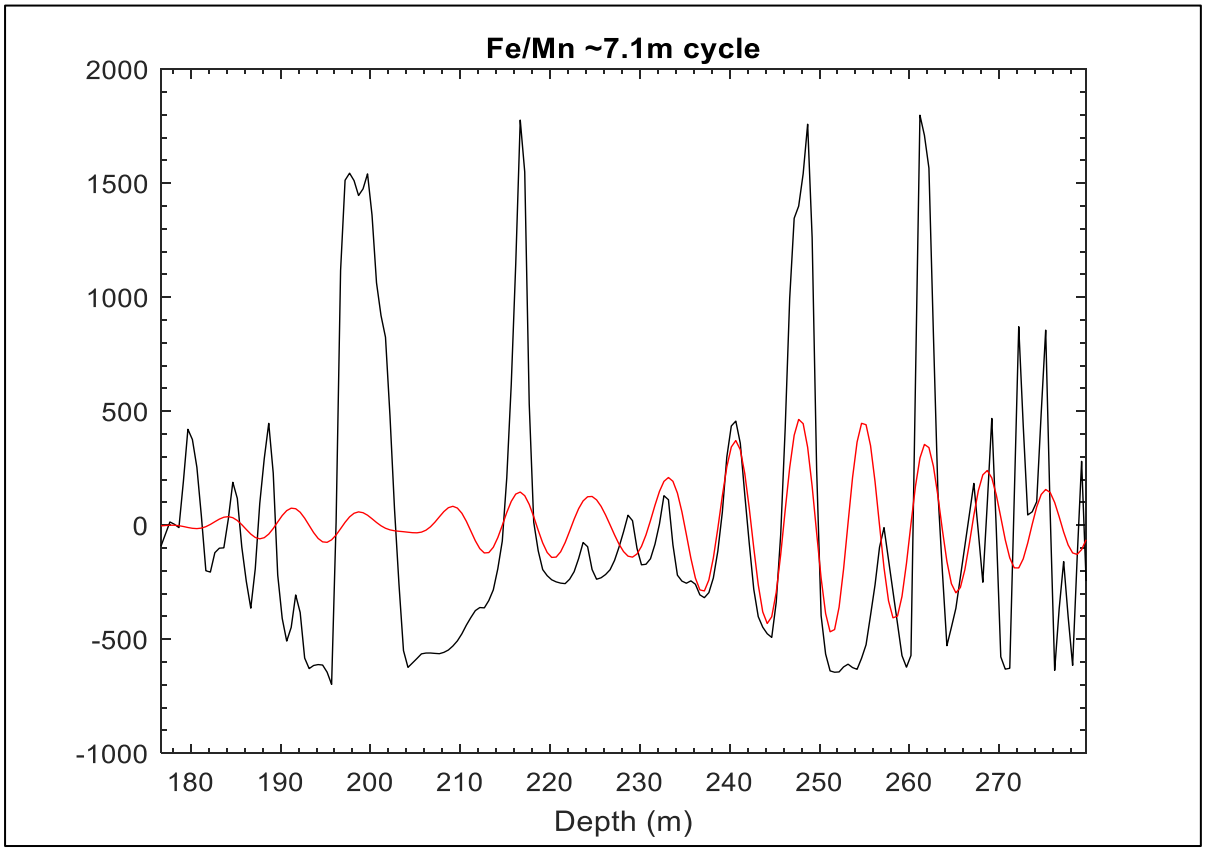

Figure 6d: The ~7.1m cycle of Fe/Mn.

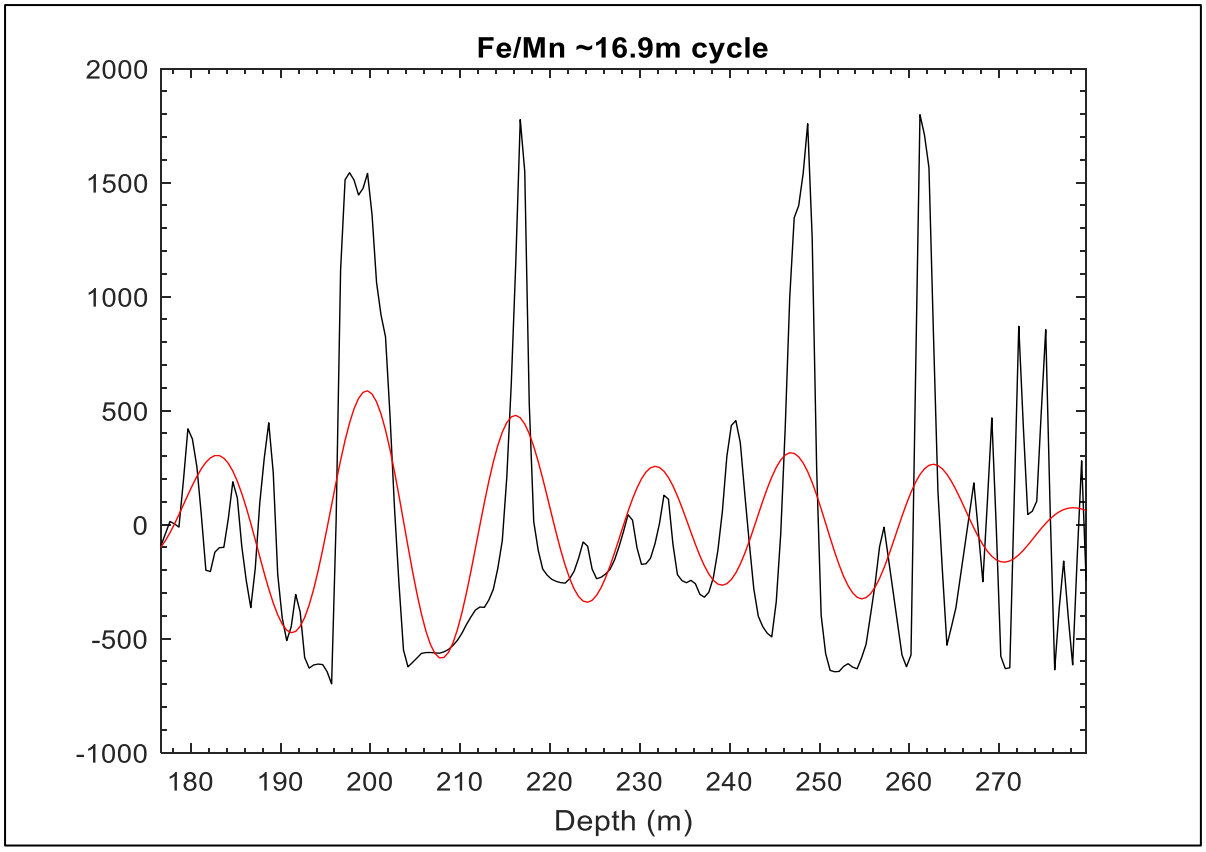

Figure 6e: The ~16.9m cycle of Fe/Mn.

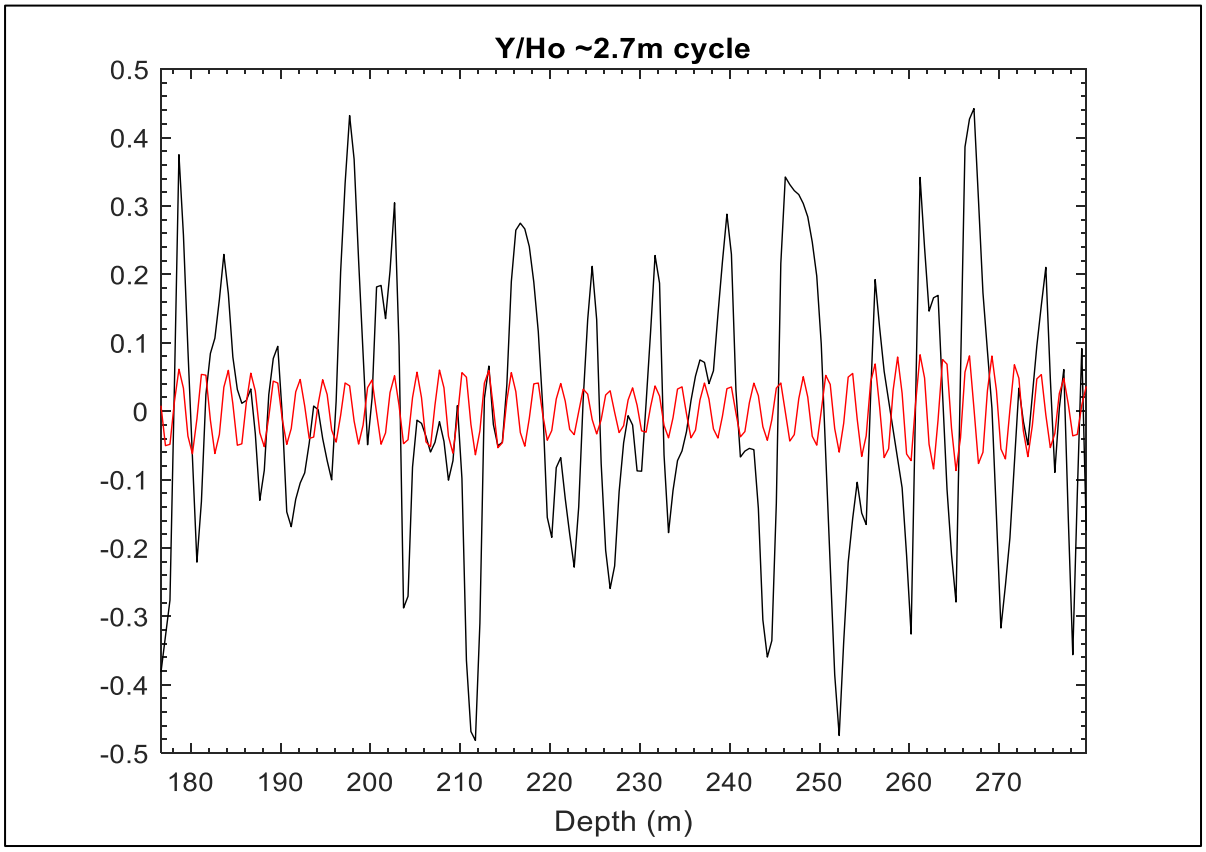

Figure 7a: The ~2.7m Y/Ho cycle.

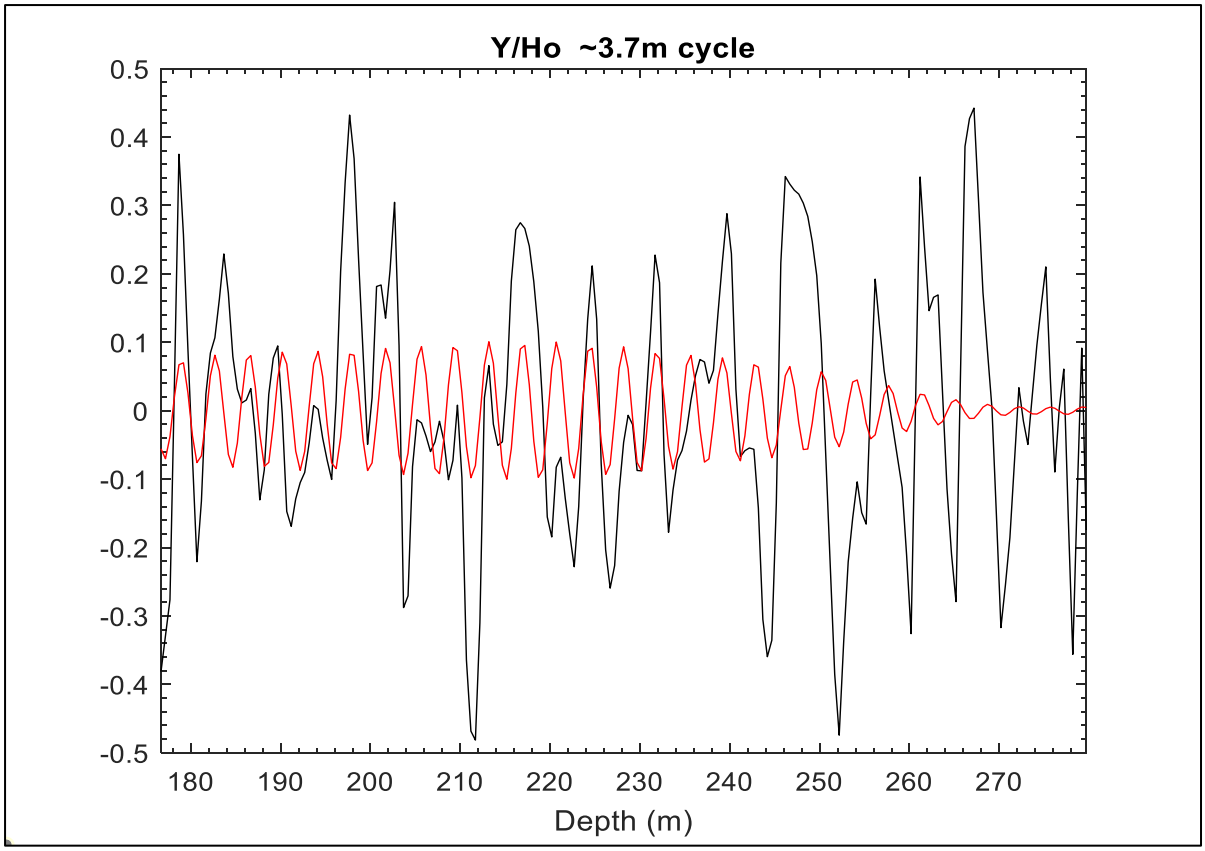

Figure 7b: The ~3.7m Y/Ho cycle.

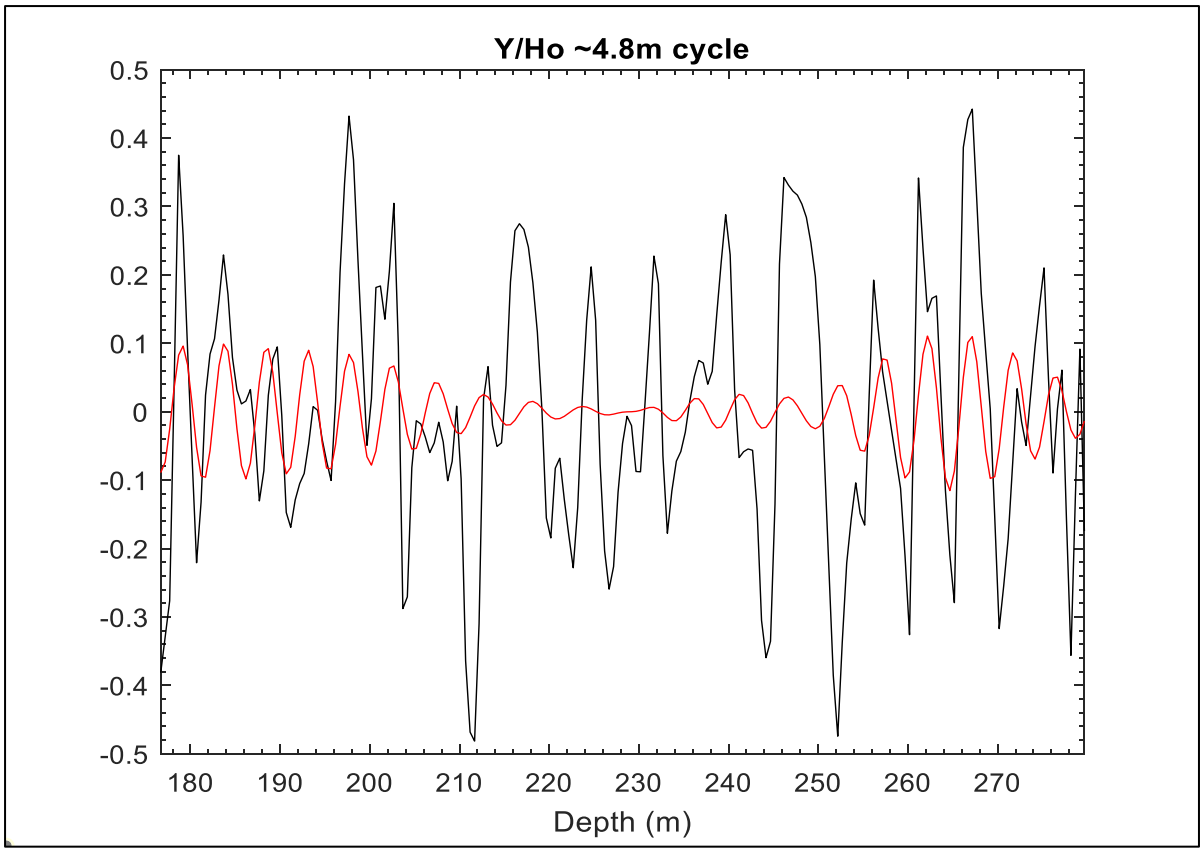

Figure 7c: The ~4.8m cycle of Y/Ho.

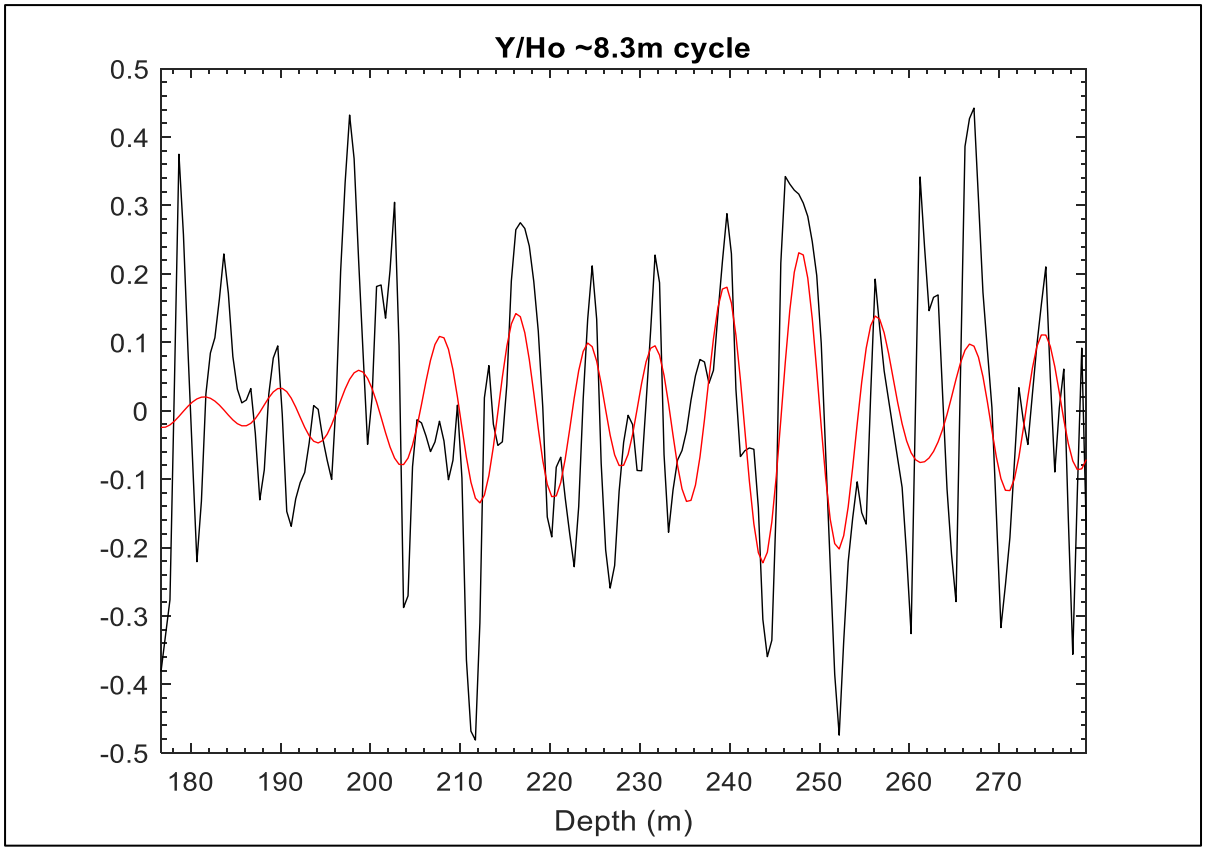

Figure 7d: The ~8.3m cycle of Y/Ho.

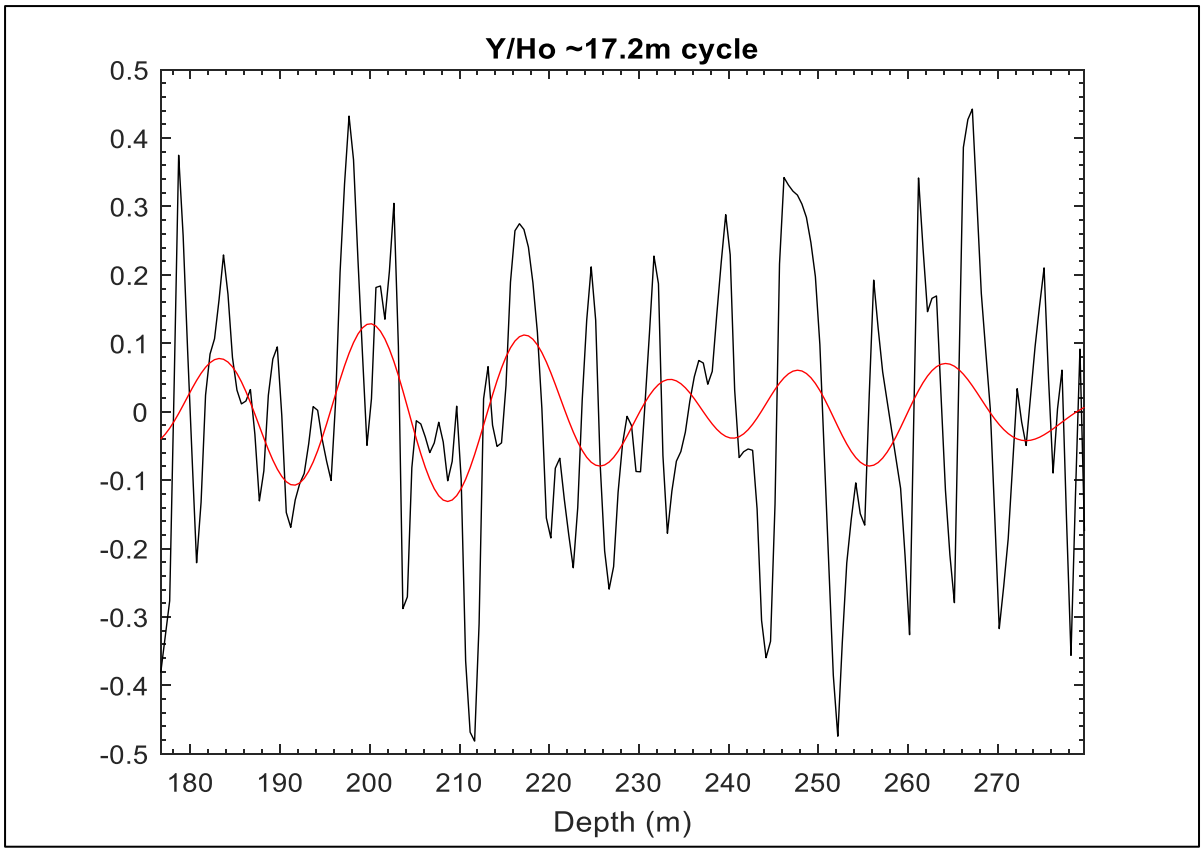

Figure 7e: The ~17.2m cycle of Y/Ho.

4. Discussion

4.1 Do the REE+Y show cyclicity?

4.1.1 Harmonics

Several recurring cycles can be observed throughout the various proxies consisting of short (~2.8m and ~3.8m), intermediate (~5.2m and ~8.0m) and long cycles (~19.5m). These three types of cycles overlap each other and together explain all observable elemental variations in the individual profiles (Figs.6 and 7, Appendix C). Several cycles are here that were not identified or highlighted in Lantink et al. (2019), namely the ~2.8m, ~3.8m and ~8.0m cycles. These cycles can be interpreted by looking at their relationship to each other and the areas in the profile they are strongest at. An important initial distinction to be made is that the shorter ~2.8m and ~3.8m cycles follow actual elemental variations and are thus not artificial harmonics (Figs.6a-b and 7a-b). The ~5.2m cycles found are the same as those found in Lantink et al. (2019), which leaves the remaining three cycles to be interpreted.

The middle interval of Y/Ho offers a concise view of the relationship between the ~3.8m and ~8.0m cycles. The 212-242m interval in figure 2 shows a double peak interval that has a consecutive step-like configuration. This configuration is comprised of a small peak followed by a larger peak. This double peak interval is captured by the ~8.0m cycle (Fig.7d), while the individual peaks are captured by the ~3.8m cycles (Fig.7b). This relationship is present in other proxies as well but is clearest in this interval. This relationship between the ~3.8m and ~8.0m cycles leads us to conclude that the ~8.0m cycle is the expressions of a double ~3.8m cycle. The ~2.8m cycle shows a similar double peak relationship to the ~5.2m cycle but is more difficult to interpret. Other than the fact that a period of ~2.8m is very close to the Nyquist frequency, the presence of a double cycle in the ~5.2m cycle would imply a ~200 Kyr cycle. While possible, this cycle is rarely if ever captured in similar cyclostratigraphic studies. The use of carbonate separation to acquire the data and the use of REE+Y might have made it possible to identify this cycle, but due to the complications with interpreting this cycle we will refrain from discussing it further.

4.1.2 Milankovitch cyclicity

The two main Milankovitch cycles identified in Lantink et al. (2019) have periods of 4.3-6.3m and 16-22m, which are cycles we have identified as well throughout all proxies studied (Figs.6 and 7, Appendix C). The coherence with the long cycle in the Y/Ho is particularly notable (Fig.5b). Besides the almost 90% coherence of the ~19.5m cycle, the cycle between 225-242m is like in the Fe/Mn the weakest cycle (Figs.6e and 7e). Dissimilar to Lantink et al. (2019), there is another significant period that occurs throughout all proxies examined, namely the ~8.0m which is a double ~3.8m cycle. The main difference between this period and the ~5.2m period is the area in the stratigraphy where the signal is the strongest. The ~5.2m cycle is strongest in the lower and sometimes upper stratigraphy (Fig.5c, Appendix C), while the ~8.0m cycle is strongest in the middle stratigraphy (Fig.5d, Appendix C). In the Fe/Mn studied we can see this as well to an extent (Fig.6). The ~8.0m signal for the middle Fe/Mn is relatively weak in the middle interval, but even with this being the case we can observe that the signals that capture this interval the best are still the ~8.0m and the ~3.8m cycle. In Lantink et al. (2019), it is theorised that the 1.2-1.6 Ma cycle is one of the main controls on compositional variation and thus sedimentation in BIFs. This combined with the observation that the weakest long cycle occurs in the middle part of the stratigraphy leads us to conclude that we are dealing with a situation where the 1.2-1.6 Ma cycle is modulating the~ 405 Kyr cycle (~5.2m). The presence of the ~8.0m cycles in the middle part of the stratigraphy and the ~5.2m cycles in the upper and lower parts would then be explained by postulating that the weak long cycle in the middle stratigraphy led to a decrease in

sedimentation. The ~3.8m cycles observed are thus a modulated ~5.2m cycle where the sedimentation rate was lower.

This theory is supported by the mineralogy when comparing the lithologies found in the upper, middle and lower stratigraphy. In figure 3 of Haddouzi (2019) we can observe that the upper and lower stratigraphy are dominated by Fe-oxides, while the middle stratigraphy is dominated by Fe-carbonates. The different lithologies most likely have different rates of deposition which directly influences the cycle thicknesses. The ~5.2m cycles are strongest in the Fe-oxide upper and lower stratigraphy, while the double ~8.0m cycles (double ~3.8m) are strongest in the middle stratigraphy. This implies that the sedimentation rate was lower in the middle stratigraphy. Furthermore, this theory explains why subsequent cycles can be of different sizes. A variable sedimentation rate implies that during relatively short periods of low deposition ~3.8m cycles would be deposited, and during regular sedimentation ~5.2m cycles. This is best illustrated in the Fe/Mn cycles (Fig.6). The 236-278m interval cannot be explained by exclusively one type of cycle. The ~5.2m cycles do not capture the peak at ~241m but captures the peak at ~257m well, while the ~8.0m cycle does the exact opposite. A combination of the ~5.2m and ~8.0m cycles along with their respective harmonics capture the entire profile for all proxies.

4.1.3 REE+Y vs Fe/Mn

The Fe/Mn record is good at capturing the long cycles but is incapable of capturing a signal in certain parts of the stratigraphy. The 204-214m interval, is a good example of this (Fig.6). The REE+Y on the other hand generally do not exhibit any areas without a distinct signal (Fig.7, Appendix C). This attribute of the REE+Y data in this study has two reasons. First is that REE+Y concentrations are much more stable over time in seawater (Bekker et al., 2014) which limits the extent of fluctuations, and the second reason is that the dataset used in this study has been corrected for mineralogy by ways of the carbonate separation procedure (Oonk et al., 2017; 2018). The signal studied in Lantink et al. (2019) is fixated on pure BIF (i.e. Fe-oxide rich BIF which are expressed in the hard ridges). Due to this, it is difficult to follow cycles in sections of the stratigraphy where pure BIF is absent like in the middle stratigraphic interval. This loss of signal does not happen in the carbonate extracted REE+Y data as it is not mineralogy dependant like Fe/Mn, nor is it influenced by other possible effects that would cause rapid changes in sedimentation. Y/Ho mirrors the Fe/Mn signal found in Lantink et al. (2019), but is better at capturing a signal regardless of position in the stratigraphy. The other REE+Y are good at capturing a signal throughout the entire stratigraphy but are not as good as Y/Ho at capturing the ~19.5m cycle.

4.2 Why do the REE+Y show cyclicity?

4.2.1 Phase relationships

There are two general phase relationships when comparing the REE+Y with the Fe/Mn, namely an (almost) in-phase relationship which is found in Y/Ho and La (Fig.5c, Appendix B) and an antiphase relationship which occurs in all other REE+Y (Appendix B). Depending on the period considered, some elements show an intermediate phase relationship though (e.g. Ce at >9m). The lag or absence thereof may be correlated to the latency time of these elements compared to the bulk rock elements (i.e. Fe and Mn). The REE+Y budget of BIFs and by extension the ocean, depends on a variety of components such as (1) continental and/or hydrothermal input (Elderfield et al., 1988; Bau et al., 1996; Bolhar et al., 2004), (2) removal of REE+Y by reactive particles (Piepgras and Jacobsen 1992; Alibo and Nozaki 1999), and (3) ocean mixing (Elderfield et al., 1988; Byrne and Kim, 1990). Removal of REE+Y from the ocean would influence the REE+Y budget instead of the speed of deposition and would thus not induce

any element-specific lag. Neither would ocean mixing, as this does not preferentially influence any element over the other. This leads to the conclusion that the lag must be related to some form of material input. While in general input of REE+Y is slower than continentally derived bulk rock material (Bekker et al., 2014), Y/Ho and La are found to more directly respond to fluctuations in continental input than the other REE+Y. Yttrium is highly enriched in seawater, which means that Y/Ho becomes more depressed with increased input of continental material (Kamber and Webb, 2001; Bolhar et al., 2004). Similarly, La-anomalies in BIF were found in Viehmann et al. (2015) to be more depressed with increased continental input. Their more direct control by continental material leads me to conclude that these elements respond more swiftly to changes in sedimentation and thus climate change when compared to the other REE+Y, leading to the in-phase relationships observed. Y/Ho and La both display the double peak sequence in the 220-244m interval (Appendix C), which furthermore supports the claim that these two proxies are controlled by similar factors.

4.2.2 REE+Y

The relationships between the REE+Y and Fe/Mn can be explained by evaluating the interplay between continental input, hydrothermal input and the scavenging of particles from the ocean budget. Among all REE+Y considered, Y/Ho best captures the Milankovitch cyclicity in the record. As stated in the previous section, Y/Ho most directly responds to changes in continental input, but it is also less prone to scavenging by reactive particles. Lanthanum, Ce and Eu have a larger ionic radius due to their lower atomic mass, which makes them more prone to adhesion to reactive particle surfaces in seawater (Planavsky et al., 2010). Y/Ho is also prone to scavenging, but not to the same extent as its ionic radius is smaller and its atomic mass greater. Furthermore, due to the relatively larger continental control compared to hydrothermal control on the Y/Ho budget of the ocean, shifts in hydrothermal activity do not interfere as much with the Y/Ho signal compared to the other REE+Y.

Among the individual REE (La, Ce and Eu), Eu exhibits the highest variability in concentrations and the least consistent signal. The strongest signals in nearly all of its cycles are found in different areas of the stratigraphy than La and Ce and are less consistent as a whole (Appendix C). This aberrant behaviour of Eu is most likely due to a larger hydrothermal input component. Europium in Pre-Cambrian seawater is highly enriched due the breakdown of plagioclase at hydrothermal systems and the subsequent input thereof into the seawater (Bau and Dulski, 1996). While the other REE+Y also have a hydrothermal component, Eu by far has the largest component from this particular source which results in a positive Eu-anomaly (Bekker et al., 2014; Konhauser et al., 2017). This strong hydrothermal component of Eu most likely interferes with the climate controlled detrital input of the other REE+Y, which causes the filtered signals to deviate from the other REE+Y. Antithetical to Eu, Y/Ho is less prone hydrothermal induced variability due to the enrichment by ways of continental input being more significant. This property might be an explanation as to why the coherency between Y/Ho and Fe/Mn is so high while the other proxies can be more variable.

4.3 Research Evaluation

We were able to quantitatively identify cyclicity in REE+Y. Agreement between the REE+Y and Fe/Mn was not ubiquitous, but this is most likely due to individual variability resulting from variable components of input and scavenging. The exact cycles varied from proxy to proxy, but the intervals wherein the cycles were found were consistent. REE+Y were found to capture signals in intervals of the stratigraphy where Fe/Mn proved insufficient. Our findings have proven that REE+Y are not only capable of capturing climatological cycles but might be better at capturing them than Fe/Mn. A ~2.7m cycle was found which is generally difficult to identify, but further analysis of this cycle is needed to verify whether we are actually dealing with a ~200 Kyr cycle. More testing is required to validate the

use of REE+Y for climatological studies, Y/Ho in particular, but these findings are very promising. The observed control of climatological cycles on REE+Y in BIFs has large implications for what we know about REE+Y systematics. These findings of consistent recurring cycles are not only a confirmation of the presence of Milankovitch cycles in BIFs, but also that climate forcings exert a primary control on REE+Y in Pre-Cambrian ocean settings. REE+Y systematics are not fully understood, but these findings will prove invaluable when studying any type of REE+Y changes through time. Corrections for climatological cycles must be made when interpreting any type of geochemical data.

5. Conclusion

Several cycles have been identified in the REE+Y which parallel the cycles found in Lantink et al., (2019). Other than the ~5.2m cycles and ~19.5m cycles which have been established previously to be the expressions of the ~405 Kyr and 1.2-1.6 Ma eccentricity cycles respectively, we have identified an additional significant cycle of ~8.0m which we have concluded to consist of two ~3.8m cycles. This ~8.0m cycle was found to be dominant in particularly the middle part of the stratigraphy where the ~19.5m cycle was the weakest in the Fe/Mn and Y/Ho. The ~3.8m cycle was found to be a modulated ~5.2m cycle where a lower sedimentation rate caused the ~5.2m cycle to be expressed as a ~3.8m cycle. The combination of the ~5.2m and ~8.0m cycles together capture the entire profile. Cycle coherency between the REE+Y and Fe/Mn was good, with Y/Ho having the highest coherence (0.71-0.91) with the Fe/Mn. All REE+Y showed an antiphase relationship with the Fe/Mn except for Y/Ho and La which were almost entirely in-phase. This phase relationship of Y/Ho and La is due to a more direct control of these elements by continental input. REE+Y were able to capture cycles in stratigraphic intervals that proved problematic for the Fe/Mn. Y/Ho showed the capacity to both capture the cycles found in our Fe/Mn and by extension those found in Lantink et al. (2019). Our findings show that REE+Y can capture climatological signals in BIFs and could prove to be a useful tool in cyclostratigraphic studies.

6. References

Alibo, Dia Sotto, and Yoshiyuki Nozaki. "Rare earth elements in seawater: particle association, shale-normalization, and Ce oxidation." *Geochimica et Cosmochimica Acta* 63.3-4 (1999): 363-372.

Bau, Michael, and Peter Dulski. "Distribution of yttrium and rare-earth elements in the Penge and Kuruman iron-formations, Transvaal Supergroup, South Africa." *Precambrian Research* 79.1-2 (1996): 37-55.

Bau, Michael, et al. "Comparison of the partitioning behaviours of yttrium, rare earth elements, and titanium between hydrogenetic marine ferromanganese crusts and seawater." *Geochimica et Cosmochimica Acta* 60.10 (1996): 1709-1725.

Bekker, Andrey, et al. "Iron formation: the sedimentary product of a complex interplay among mantle, tectonic, oceanic, and biospheric processes." *Economic Geology* 105.3 (2010): 467-508.

Bekker, At, et al. "Iron formations: Their origins and implications for ancient seawater chemistry." *Treatise on geochemistry*. Vol. 12. Elsevier, 2014. 561-628.

Bolhar, Robert, et al. "Characterisation of early Archaean chemical sediments by trace element signatures." *Earth and Planetary Science Letters* 222.1 (2004): 43-60.

Byrne, Robert H., and Ki-Hyun Kim. "Rare earth element scavenging in seawater." *Geochimica et Cosmochimica Acta* 54.10 (1990): 2645-2656.

Elderfield, Henry, et al. "Rare earth element geochemistry of oceanic ferromanganese nodules and associated sediments." *Geochimica et Cosmochimica Acta* 45.4 (1981): 513-528.

Elderfield, Henry, et al. "Rare earth element geochemistry of oceanic ferromanganese nodules and associated sediments." *Geochimica et Cosmochimica Acta* 45.4 (1981): 513-528. Elderfield, Henry. "The oceanic chemistry of the rare-earth elements." *Philosophical Transactions of the Royal Society of London. Series A, Mathematical and Physical Sciences* 325.1583 (1988): 105-126.

Haddouzi, Appie. "A high-resolution geochemical analysis of the Kuruman Banded Iron Formation: The identification of significant meter-scale variability in REE+Y." 2019.

Kamber, Balz S., and Gregory E. Webb. "The geochemistry of late Archaean microbial carbonate: implications for ocean chemistry and continental erosion history." *Geochimica et Cosmochimica Acta* 65.15 (2001): 2509-2525.

Konhauser, Kurt O., et al. "Iron formations: A global record of Neoarchaean to Palaeoproterozoic environmental history." *Earth-Science Reviews* 172 (2017): 140-177.

Lantink, Margriet, et al. "Milankovitch cyclicity in Paleoproterozoic BIF of the Kuruman Iron Formation in South Africa." *Geophysical Research Abstracts*. Vol. 21. 2019.

Li, Mingsong, Linda Hinnov, and Lee Kump. "Acycle: Time-series analysis software for paleoclimate research and education." *Computers & geosciences* 127 (2019): 12-22.

Oonk, Paul Bernardus Hendrikus. Fraction-specific geochemistry across the Asbestos Hills BIF of the Transvaal Supergroup, South Africa: implications for the origin of BIF and the history of atmospheric oxygen. Diss. Rhodes University, 2017.

Oonk, P. B. H., et al. "Fraction-specific rare earth elements enable the reconstruction of primary seawater signatures from iron formations." *Geochimica et Cosmochimica Acta* 238 (2018): 102-122.

Paillard, Didier, L. D. Labeyrie, and Pascal Yiou. "AnalySeries 1.0: a Macintosh software for the analysis of geophysical time-series." *Eos* 77.39 (1996): 379.

Piepgras, Donald J., and Stein B. Jacobsen. "The behavior of rare earth elements in seawater: Precise determination of variations in the North Pacific water column." *Geochimica et Cosmochimica Acta* 56.5 (1992): 1851-1862.

Planavsky, Noah, et al. "Rare earth element and yttrium compositions of Archean and Paleoproterozoic Fe formations revisited: new perspectives on the significance and mechanisms of deposition." *Geochimica et Cosmochimica Acta* 74.22 (2010): 6387-6405.

Thomson, D. J. (1982). Spectrum estimation and harmonic analysis. *Proceedings of the IEEE*, *70*(9), 1055-1096.

Viehmann, Sebastian, et al. "Geochemistry of the Krivoy Rog Banded Iron Formation, Ukraine, and the impact of peak episodes of increased global magmatic activity on the trace element composition of Precambrian seawater." *Precambrian Research* 270 (2015): 165-180.